HHS Public Access

Author manuscript

Neuroimage. Author manuscript; available in PMC 2016 November 15.

Published in final edited form as:

Neuroimage. 2015 November 15; 122: 114–130. doi:10.1016/j.neuroimage.2015.08.019.

Microscale Spatiotemporal Dynamics during Neocortical Propagation of Human Focal Seizures

Fabien B. Wagner[1], **Emad N. Eskandar**[9,10], **G. Rees Cosgrove**[4,6], **Joseph R. Madsen**[11,12], **Andrew S. Blum**[3], **N. Stevenson Potter**[3], **Leigh R. Hochberg**[2,5,7,8,13], **Sydney S. Cash**[8], and **Wilson Truccolo**[1,5,7]

[1]Department of Neuroscience, Brown University, Providence, RI, 02912

[2]School of Engineering, Brown University, Providence, RI, 02912

[3]Department of Neurology, Alpert Medical School, Brown University, Providence, RI, 02912

[4]Department of Neurosurgery, Alpert Medical School, Brown University, Providence, RI, 02912

[5]Institute for Brain Science, Brown University, Providence, RI, 02912

[6]Norman Prince Neurosciences Institute, Brown University, Providence, RI, 02912

[7]Center for Neurorestoration and Neurotechnology, Department of Veterans Affairs, Providence, RI

[8]Department of Neurology, Massachusetts General Hospital and Harvard Medical School, Boston, MA, 02114

[9]Department of Neurosurgery, Massachusetts General Hospital and Harvard Medical School, Boston, MA, 02114

[10]Nayef Al-Rodhan Laboratories for Cellular Neurosurgery and Neurosurgical Technology, Massachusetts General Hospital and Harvard Medical School, Boston, MA, 02114

[11]Department of Neurosurgery, Children's Hospital and Harvard Medical School, Boston, MA, 02114

[12]Department of Neurosurgery, Brigham and Women's Hospital, Harvard Medical School, Boston, MA, 02114

[13]Department of Neurology, Brigham and Women's Hospital, Harvard Medical School, Boston, MA, 02114

Abstract

Some of the most clinically consequential aspects of focal epilepsy, e.g. loss of consciousness, arise from the generalization or propagation of seizures through local and large-scale neocortical

Corresponding authors: Fabien Wagner and Wilson Truccolo, fabien.wagner@epfl.ch; wilson_truccolo@brown.edu.

Conflict of interest: none.

networks. Yet, the dynamics of such neocortical propagation remain poorly understood. Here, we studied the microdynamics of focal seizure propagation in neocortical patches (4 × 4 mm) recorded via high-density microelectrode arrays (MEAs) implanted in people with pharmacologically resistant epilepsy. Our main findings are threefold: (1) A newly developed stage segmentation method, applied to local field potentials (LFPs) and multi-unit activity (MUA), revealed a succession of discrete seizure stages, each lasting several seconds. These different stages showed characteristic evolutions in overall activity and spatial patterns, which were relatively consistent across seizures within each of the 5 patients studied. Interestingly, segmented seizure stages based on LFPs or MUA showed a dissociation of their spatiotemporal dynamics, likely reflecting different contributions of non-local synaptic inputs and local network activity. (2) As previously reported, some of the seizures showed a peak in MUA that happened several seconds after local seizure onset and slowly propagated across the MEA. However, other seizures had a more complex structure characterized by, for example, several MUA peaks, more consistent with the succession of discrete stages than the slow propagation of a simple wavefront of increased MUA. In both cases, nevertheless, seizures characterized by spike-wave discharges (SWDs, ~ 2–3Hz) eventually evolved into patterns of phase-locked MUA and LFPs. (3) Individual SWDs or gamma oscillation cycles (25–60 Hz), characteristic of two different types of recorded seizures, tended to propagate with varying degrees of directionality, directions of propagation and speeds, depending on the identified seizure stage. However, no clear relationship was observed between the MUA peak onset time (in seizures where such peak onset occurred) and changes in MUA or LFP propagation patterns. Overall, our findings indicate that the recruitment of neocortical territories into ictal activity undergo complex spatiotemporal dynamics evolving in slow discrete states, which are consistent across seizures within each patient. Furthermore, ictal states at finer spatiotemporal scales (individual SWDs or gamma oscillations) are organized by slower time-scale network dynamics evolving through these discrete stages.

Keywords

epilepsy; collective dynamics; secondary generalization; cortical waves; neural state segmentation

INTRODUCTION

Epilepsy is one of the major neurological disorders affecting about 65 million people worldwide (Thurman et al., 2011). In the specific case of focal epileptic seizures, seizures appear to initiate in a localized region (seizure focus) and then spread or propagate to other brain areas via local and large-scale network interactions. In particular, large spread throughout neocortical areas, clinically referred to as secondary generalization to distinguish it from primarily generalized seizures, can be the crucial event leading to loss of consciousness or impairment in motor or language function. Despite its importance, neocortical propagation of focal seizures remains poorly understood. Advances in this front could lead to new therapies based on early seizure detection followed by guided drug delivery or electrical stimulation to prevent spread (Morrell, 2011). In addition, the problem is also relevant for the general understanding of multiscale neural dynamics in neocortical networks.

Recent advances in MEA recordings have opened a new window into seizure propagation by allowing the simultaneous recordings of ensembles of single unit activity (SUA), localized multiunit activity (MUA) and high-density spatial local field potentials (LFPs) over neocortical patches during seizures in people with intractable epilepsy (Keller et al., 2010; Truccolo et al., 2011, 2014; Schevon et al., 2008, 2012). Schevon et al. (2012) addressed seizure propagation in neocortical patches by examining how peaks in MUA rate evolved in time and space during seizures. In some of the patients, where the MEA was away from the putative seizure onset area, they observed that the peak in MUA slowly traveled across the MEA. Their main proposed hypothesis is that this slow MUA-peak propagation reflects an ictal wavefront advancing over areas under a feedforward inhibitory veto ("penumbra" areas), which needs to be broken in order for a distal area to be recruited into the ictal state.

Here, we adopted an approach to segment and track the evolution of different seizure stages based on several MUA and LFP features, not only MUA peaks. The focus is on MUA, instead of single neuron spiking activity (Truccolo et al., 2011, 2014), since the former more easily relates to the bulk population activity. We examined the time evolution of all of these features and corresponding stages on 4 mm × 4 mm neocortical patches recorded via 96-channel MEAs in 5 patients. Etiologies consisted of four cases of mesial temporal sclerosis and one case of cortical dysplasia. Recorded patches included middle or superior temporal gyri. In all these cases, the MEA was implanted in an area outside the putative seizure onset zone, such that the ictal activity examined here required propagation.

Our results indicate that seizures spread through a succession of discrete stages characterized by specific and reproducible spatiotemporal dynamics occurring at the timescale of seconds. These dynamics involved, in some of the seizures, the propagation of what appeared to be a slow wavefront as observed previously by others (e.g. Schevon et al. 2012). However, in several other seizures this phenomenon was not observed, even though the related neural dynamics showed clear features of ictal states (e.g. MUA-LFP phase-locking during 2–3Hz spike-wave discharges). Finally, depending on the seizure type, these stages influenced the propagation patterns of individual spike-wave discharges (SWDs) or gamma oscillations, which occurred at a finer time resolution.

MATERIALS AND METHODS

Patients and Clinical/Research MEA Recordings

Research was approved by local Institutional Review Boards at Massachusetts General Hospital/Brigham and Women's Hospitals (Partners Human Research Committee) and at Rhode Island Hospital. Five patients with pharmacologically intractable focal epilepsy freely consented to the study. These patients underwent neuromonitoring for seizure localization and functional assessment of neocortical areas via standard clinical recordings based on subdural electrocorticograms (ECoGs), strip electrodes, and depth electrodes placed in subcortical structures, as decided by a clinical team completely independent from this research. Following the clinical team's decision, patients were contacted by the research team. The five patients in this study (P1-P5) were implanted for a period of 5–14 days with an additional 10 × 10 (4 mm × 4 mm) NeuroPort MEA (Blackrock Microsystems, Utah; Hochberg et al., 2006; Schevon et al., 2008; Truccolo et al., 2008; Waziri et al., 2009;

Truccolo et al., 2011) in a neocortical area expected to be resected with high probability, in either the middle (P1, P3, P4, P5) or superior (P2) temporal gyrus. This research probe consisted of 96 recording platinum-tipped silicon probes, with a length of either 1-mm (P4, P5) or 1.5-mm (P1, P2, P3), corresponding to neocortical layer III as confirmed by histology after resection. Seizures were identified by experienced encephalographers (S.S.C. and A.S.B.) via inspection of ECoGs and clinical manifestations recorded in video. Seizure onsets were detected ~2 cm (P1, P4, P5) or ~3 cm (P2 and P3) away from the research MEA, based on the clinical ECoG electrodes. These recordings were therefore outside the seizure-onset zone. Details of the clinical cases and seizures are given below. These data have been previously used in another study (Truccolo et al., 2014). Participants 1 to 5 in that earlier study correspond here to patients P5, P3, P2, P4 and P1 respectively.

Patient P1 (mesial temporal sclerosis)—Patient P1 was a 45-year-old right-handed man at the time of his surgery, with a history of medically refractory focal seizures which included impairment of consciousness and observable motor components. Specifically, his seizures lasted 1–2 minutes, started with arousal and bilateral arm/leg extension, followed by leftward head deviation, left arm flexion, and generalized tonic-clonic activity. He underwent placement of grids, strips and depths over the right hemisphere. During secondary generalization, the seizures spread to the location of the NeuroPort MEA in the middle temporal gyrus and beyond. The MEA site was in the irritative zone, but not in the epileptogenic lesion. It was not clear whether the site was in the symptomatogenic zone. The patient underwent a right temporal lobectomy and has remained seizure-free for 4 years while on medications (ILAE surgical outcome scale 1, last update 28 months post surgery).

Patient P2 (mesial temporal sclerosis)—Patient P2 was a left-handed, 32-year-old man at the time of his surgery, with a history of pharmacologically intractable focal seizures which included impairment of consciousness, autonomic and motoric components. Seizures began when he was 10 years old. His seizures were characterized by sudden onset of nonsensical speech followed by staring and unresponsiveness with head turning to the right, automatisms, and posturing involving the right more than left arm and hand. These spells lasted ~ 1–2 min. MRI suggested left (dominant) temporal polymicrogyria. He underwent placement of grids and strips to delineate the seizure focus with respect to this area of abnormal sulcation. Seizures were found to emanate from the mesial temporal structures (including the MEA implant site) and beyond. The MEA site was not in the epileptogenic lesion or in the irritative zone. It was not clear whether the site was in the symptomatogenic zone. The patient underwent a left temporal lobectomy. Histology showed extensive sclerosis in hippocampus and mild gliosis with no evidence of cortical dysplasia in the microelectrode implant site. He has been seizure-free for 3.5 years (ILAE surgical outcome scale 1, last update 40 months post surgery).

Patient P3 (cortical dysplasia)—Patient P3 was a 25-year-old, left-handed woman at the time of her 7 d phase II video-EEG study. Her seizures began at age 14 and were medically intractable focal seizures which included some impairment of awareness and autonomic components. Her events began with an aura of nausea and/or a “tunneling” sensation, then a flattening of affect, slowed responsiveness, automatisms, and associated

amnesia. These occurred three to four times per month and were persistent despite a three-drug anticonvulsant regimen. MRI revealed an extensive nodular gray matter heterotopia (cortical dysplasia) in the right hemisphere. Phase I LTM had found right hemispheric onset seizures and fMRI had shown normal left-sided language activation patterns and normal motor activation patterns. Wada testing confirmed left hemispheric language dominance and suggested her left hemisphere could adequately support memory function subsequent to a right temporal lobectomy. Recorded seizures lasted between ~ 1 and 2.5 min each and began in the right middle and upper gyri of the posterior temporal cortex. The patient underwent an extensive right temporal resection with extension posteriorly toward the right temporo-occipital junction but sparing of much of the mesial temporal structures (including the hippocampus). Histology revealed subtle neuronal dysgenesis and focal superficial gliosis and areas of encephalomalacia in the posterior temporal neocortex, including the recorded seizure-onset zone. Histology of the microelectrode implant site showed mild gliosis. The MEA site was not in the epileptogenic lesion. It was not clear whether the site was in the symptomatogenic zone. The irritative zone in this patient was not defined, as we did not have an official ECoG report discussing the location of interictal discharges. The patient has remained seizure free for 3 years since the resection (ILAE surgical outcome scale 1, last update 37 months post surgery).

Patient P4 (mesial temporal sclerosis)—Patient P4 was a 21-year-old, right-handed man whose seizures began at the age of 15. His seizures were characterized by a blank stare and oral automatisms accompanied by stiffening and posturing of the right hand consistent with an intractable focal seizure with impairment of awareness and observable motor components. While his MRI was unremarkable, his semiology and phase I recordings suggested a left temporal onset. All seizures had similar clinical and electrographic signatures with a left gaze preference at onset followed by tonic and then clonic movements of the right arm. The patient underwent a left temporal lobectomy. Histology showed gliosis and moderate neuronal loss in regions CA4 and CA3 of the hippocampus, and mild dysplastic changes in the microelectrode implant site. The MEA site was likely in the epileptogenic lesion based on post-operative histology, but not in the irritative zone. It was not clear whether the site was in the symptomatogenic zone. He has remained seizure-free for 4 years after surgery (ILAE surgical outcome scale 1, last update 46 months post surgery).

Patient P5 (mesial temporal sclerosis)—Patient P5 was a 52-year-old, right-handed woman at the time of surgery, who began having seizures at the age of 4. At the time of electrode implantation she was having an average of 10–15 seizures per day associated with impaired consciousness, motoric components which could evolve to bilateral convulsive events involving tonic and clonic components. Her seizures usually started with sudden speech arrest and were accompanied by confusion and repetition of the activity she was doing just before the onset of the seizure. MRI showed a large lesion in the left hemisphere extending from the occipital region to the temporal region, which was consistent with encephalomalacia. A positron emission tomography scan showed hypometabolism in the left occipital, temporal, and parietal regions. Recorded seizures lasted approximately a minute or less. The patient underwent resection of the left anterior temporal lobe. Histology revealed

hippocampal sclerosis with secondary cortical gliosis and normal cortical layering (no evidence of dysplasia) with focal gliosis in superficial layers in the microelectrode implant site. The MEA site was in the epileptogenic lesion and in the irritative zone. It was not clear whether the site was in the symptomatogenic zone. The patient was initially seizure free for one year after resection (ILAE surgical outcome scale 1), but then seizures resumed at a significantly lower frequency (ILAE surgical outcome scale 4, 68 months post-surgery).

Data Analysis

Seizure inclusion criteria, terminology and seizure onset times—Analyses were performed in all 5 patients who participated in this study. In each patient, we analyzed seizures that had been previously identified by encephalographers in the clinical teams. The total number of seizures in each patient was: 3, 2, 3, 2, 3 in P1 to P5 respectively. Among these 5 patients, 4 of them had so-called “spike-wave seizures,” while 1 patient (P5) had seizures characterized by a high power in the gamma range and referred to as “gamma seizures” (Truccolo et al., 2014). Identification of electrographic (i.e. based on iEEG) and clinical seizures was done blindly and independently as part of the clinical procedures adopted at Massachusetts General Hospital, Brigham and Women’s Hospitals and Rhode Island Hospital. In addition, seizure onset time at the MEA recording site was determined based on visual inspection of the MEA data as the time when the first epileptiform discharge could be seen in the LFPs. Since we focus here on the segmentation of ictal stages during the early propagation at the MEA site, we set time 0 in all figures and analyses as the seizure onset time based on the MEA recordings.

LFP and MUA signal processing—Recordings were performed with the 96-channel MEA NeuroPort system (BlackRock Microsystems, Utah; Hochberg et al., 2006; Schevon et al., 2008; Truccolo et al., 2008, 2010, 2011, 2014). Electric potentials were recorded broadband (0.3–7.5k Hz, analog filtering) and sampled at 30 kHz. LFPs and MUA were then extracted offline from these raw data. LFPs were filtered between 0.3 and 300 Hz (3^{rd}-order Butterworth filter, applied forward-backward to avoid phase distorsion). In one patient (P4), we also used a notch filter at 60 Hz (2^{nd}-order Infinite Impulse Response notch filter with a Q-factor of 35) to remove excessive line noise. The resulting LFP signal was then downsampled at 1 kHz.

MUA was obtained by high-pass filtering the raw data above 300 Hz (3^{rd}-order forward-backward Butterworth filter). The resulting signal was then thresholded and event counts were binned to yield the rate of thresholded MUA (referred to as MUA rate). Specifically, an event was detected every time the high-pass MUA crossed a threshold located 4 standard deviations below or above the mean (mean and standard deviations computed during a 15-s baseline period preceding each seizure). The MUA rate was then defined as the rate of these events in overlapping sliding time bins of either 1 s or 20 ms, shifted every 100 ms.

Electrode selection and artifact removal—For each seizure independently, we excluded from the LFP/MUA analyses all electrodes with excessive movement artifacts or line noise during the seizure. Additionally, we excluded from the MUA analyses the electrodes with an abnormally low MUA event rate/amplitude, as assessed by visual

inspection. The total number of excluded electrodes ranged between 0 and 19% across patients and seizures. When movement artifacts were minor or occurred towards the end of/after the seizure, we removed them by clipping high-amplitude values in a time window adapted to each seizure (typically a 1-s window for LFPs, and a 150-ms window for MUA, centered on the artifact in both cases). Occasionally, we removed a transient period of high-amplitude line noise in the MUA by computing the MUA envelope (MUA low-pass filtered below 1 Hz) and clipping the values at all time points where the envelope exceeded a certain threshold. Note that artifact removal at the end of the seizures did not affect our analyses, which were mainly focused on the seizure early propagation period.

Spectrograms—Spectrograms were computed from the LFPs between 0 and 90 Hz, using a 1-s sliding time window shifted every 100 ms, and a multitaper method based on 3 tapers and a time half-bandwidth product TW = 2. The multitaper method was implemented via the Chronux toolbox (http://chronux.org/; Mitra and Bokil, 2007) using the 'mtspecgramc' function. The number of tapers was chosen to obtain a reasonable degree of smoothness while maintaining enough band separation. All spectrograms are represented in dB with a reference level of 1 $\mu V^2/Hz$.

LFP/MUA feature extraction—As an input to the segmentation algorithm described next, we used features derived from either LFPs or MUA. For MUA features, we considered the rate of thresholded MUA in 1-s bins, as described in the section "LFP and MUA signal processing". A feature vector of dimension equal to the number of electrodes was therefore obtained every 100 ms, based on MUA data in a 1-s window centered on the current time step.

Another set of features, based on LFPs, consisted of the spectral power in 6 different frequency bands (delta: 0–2 Hz, theta: 2–8 Hz, alpha: 8–14 Hz, beta: 14–30 Hz, low-gamma: 30–60 Hz, mid-gamma: 60–90 Hz) for each electrode. These features were obtained at each time step by integrating over frequencies the power (in dB) computed in the spectrogram, using linear interpolation between the discrete values calculated with the multitaper method (see section "Spectrograms"). A feature vector of dimension "6 x number of electrodes" was therefore obtained every 100 ms, based on LFP data in a 1-s window centered on the current time step.

Segmentation algorithm—We developed a semi-automatic algorithm capable of segmenting a time series into distinct stages under the assumption that samples within the same stage have more similar features than samples across two consecutive stages. Features were derived from either LFPs or MUA as described above and used to compute a pairwise distance (or "dissimilarity") matrix between all time samples (examples are shown in Fig. 2). The distance between two time samples was defined as the Manhattan distance between their feature vectors (the Manhattan distance was preferred over the Euclidean distance because it is more robust in high dimensions). Under our assumption, the structure of this distance matrix should reveal the segmentation of the underlying time series. Pairwise distances within the same stage should be smaller than pairwise distances across two consecutive stages, resulting in a diagonal block structure. We designed an algorithm able to semi-automatically find this block structure. Each time step was assigned a score

representing its separating/discriminative power between two consecutive blocks. Since the size of the block is originally unknown (and given that segmentation is potentially a multi-scale problem), we tested the separating power at each time step for blocks of various sizes. More precisely, for each time step t and integer k, we considered the sub-matrix of size 2k+1 centered at time t. If we call A and B the k indices respectively before and after t, this sub-matrix is simply $\begin{pmatrix} D_{AA} & D_{AB} \\ D_{AB} & D_{BB} \end{pmatrix}$, where D_{AA} and D_{BB} are the within-block distance matrices for the k indices respectively before and after t, and D_{AB} is the between-block distance matrix between the k indices before and the k indices after t. The score at time t and scale k was then defined as $\frac{2\times mean(D_{AB})}{mean(D_{AA})+mean(D_{BB})}$, a measure similar to a clustering index. Importantly, the size k of the matrices D_{AA}, D_{BB} and D_{AB} determines the temporal resolution at which the segmentation is performed. We varied k from values corresponding to 20 s down to about 3 s. For each scale k, we identified the peaks of the score function over time by their prominence, i.e. the minimum vertical distance that the signal must descend on either side of the peak before climbing back to a level higher than the peak. Since each stage boundary can be seen at several consecutive scales, we considered only the scale where the peak prominence was most pronounced. This was performed by keeping track of peaks identified at previous scales and identifying two peaks as the same when they occurred within a certain time window (2.5 s). Peak prominences across time and scales were then sorted, so that peaks with the highest prominence were selected first. The last step was manual, based on visual inspection of the data: among the list of sorted peaks, a human observer decided how far the segmentation should go, i.e. what the smallest acceptable peak prominence should be.

Analysis of spatial pattern evolution: intensity variations and cumulative cosine distance—To characterize the evolution over time of specific spatial patterns (Figs. 5 and 7), we separated the contributions of overall intensity variations and spatial reorganization. Each spatial pattern (of MUA rate or LFP power) was represented by a vector where each component corresponds to one electrode. The spatial reorganization between two patterns/stages was quantified as the cosine distance between the two vectors (as used previously e.g. by Cacioppo et al., 2014). The cosine distance does not take into account the norm of the vectors, but only the “angle” they form in a high-dimensional space. Therefore, if two patterns are a scaled version of one another, differing only in overall intensity, their cosine distance is 0. To complement the use of the cosine distance, we also compared the mean intensity (i.e. mean MUA rate or mean LFP power) across electrodes between the two patterns. Together, these two measures (change in mean intensity and cosine distance) yield a complete representation of the changes that occur between two patterns. Since we looked at patterns occurring during multiple seizure stages, we adapted this representation to look at the evolution of these changes over time. Specifically, we computed the cosine distance between each stage and the preceding one, and plotted the evolution of the cumulative cosine distance over time. We complemented this measure with the evolution of the mean intensity over time, yielding a 2-dimensional “trajectory” representing the changes occurring across stages. Note that the cumulative cosine distance

increases monotonically over time, and that this representation does not depend explicitly on the duration of each stage, but rather represents a "signature" of seizure evolution.

Analysis of discharge and gamma oscillation propagation—We aimed at characterizing the propagation of LFP/MUA discharges and gamma oscillations occurring during each stage of the seizure. Briefly, we detected individual events (discharges or gamma oscillations), computed the delay map associated with each of these events, characterized their directionality index, direction of propagation and speed, and finally pooled the data together across all events. Events were detected as peaks in the electrode-averaged signal, with a prominence above a certain threshold. For spike-wave seizures, we selected discharges in the LFPs (respectively MUA rate) as negative (respectively positive) peaks with a prominence of at least 1.5–2 (respectively 0.5) standard deviations. For gamma seizures, we examined both low-frequency discharges (< 10 Hz) in LFPs, and gamma oscillations (25–60 Hz) in the LFPs and MUA rate (based on an initial visual inspection of the data). Low-frequency LFP discharges were identified as positive peaks with a prominence of at least 2.3 standard deviations. For gamma oscillations, the signals (LFPs and MUA rate) were filtered in a narrow band (25–60 Hz), taking advantage of their quasi-sinusoidal amplitudes so that any point could be used as a reference. We considered local maxima with no condition on the prominence.

Once the event time was identified, we searched the local extrema on each electrode in a time window of 40 ms centered on the potential event population activity, yielding a delay map of the event. Activity in missing or excluded electrodes was estimated via linear interpolation. The delay gradient of this delay map was then computed. Next, we defined the directionality index, which represents how directional an event propagates, as the norm of the mean delay gradient divided by the mean of the norm of the delay gradient: $D.I. = \frac{\|\langle \nabla \tau \rangle\|}{\langle \|\nabla \tau\| \rangle}$, similarly to the definition by Hatsopoulos et al. (2006), but applied to the delay map τ instead of the phase map. Based on visual assessment of the data, we decided that events with a directionality index above 0.2 showed enough directionality to perform a more detailed spatiotemporal analysis. For these events, we computed their direction of propagation, defined as the direction of the mean delay gradient. We also computed statistics across events. Mean delay maps (Figs. 8 and 9), were obtained by averaging delays on each electrode across all events with a directionality index above 0.2. For the directions of propagation, we took the circular average of the directions of propagation of each event, weighted by the corresponding directionality indices. Since taking the circular average only makes sense when the directions of propagation are distributed unimodally, we reported the average direction of propagation when the resulting average had a norm above 0.2 (for consistency with the threshold value used for the directionality index). Similarly, we reported mean delay maps only when the average propagation vector had a norm above 0.2. We also calculated the inverse of the speed for each event with a directionality index above 0.2. To compute the average speed across events, we first computed the average of the inverse of the speed, and then inverted it, to prevent the events with almost no propagation (delays close to 0 leading to ~ infinite speed) to dominate the average.

RESULTS

A subset of spike-wave seizures are characterized by a transient increase in MUA which happens tens of seconds after local seizure onset

We first tested the hypothesis of a propagating ictal wavefront characterized by a moving peak in MUA, as examined previously by Schevon et al. (2012). Their analysis was replicated using the rate in 20-ms bins of threshold crossings in the high-pass MUA (Fig. S1). Because the focus here is on the evolution of ictal stages during early propagation at the area recorded by the MEA, time 0 in all of the following analysis and figures corresponds to the seizure onset time based on MEA recordings (Materials and Methods). We observed that in some spike-wave seizures (e.g. Fig. S1A), the initial seizure period showed an overall increase in MUA rate, which occurred at a slower time scale than in individual epileptic discharges seen in both LFPs and MUA. Because of this slow time scale, 1-s time bins (instead of 20-ms) were used to identify the time at which the MUA rate reached a maximum (Fig. 1). In patient P1, the peak of MUA rate occurred at a different time on each electrode (Fig. 1A, P1) and the relative delays of this peak were spatially organized (Fig. 1B, P1), supporting the idea a propagating ictal wavefront as described by Schevon and colleagues. However, the presence of an ictal wavefront was not as clear in other patients. In patient P2 for example, some electrodes showed two peaks in the MUA rate, while other electrodes were only affected by either the first or the second peak (Fig. 1A, P2), and the relative delays of the highest peak on each electrode had an unclear spatial organization (Fig. 1B, P2). Similarly, the MUA rate in patient P3 seemed to possess an underlying structure more complex than a single ictal wavefront. Moreover, in one seizure from this patient, the peak of MUA rate occurred towards the end of the seizure on several electrodes (Fig. 1A, P3, seizure 1). Additionally, the patterns of MUA seen during this entire seizure (P3, seizure 1) seemed to be the same as those observed during the initial period of the other seizures from the same patient (e.g. P3, seizure 2). Overall, the observations in patients P2 and P3 suggested that the early propagation of these seizures was more complex than the propagation of a single planar wavefront of increased spiking activity. To further and more accurately describe this period of early propagation, we decided to verify the hypothesis of successive discrete stages occurring shortly after local seizure onset, and to analyze their reproducibility within patients. We achieved this by comparing all clinical seizures within each patient using a newly developed neural state segmentation approach.

All spike-wave and gamma seizures evolve through discrete stages of spatiotemporal MUA and LFPs, which remain consistent within each patient for tens of seconds after local seizure onset

To identify the presence of different stages occurring during seizure initiation and early propagation, we developed a semi-automatic segmentation algorithm based on either LFPs or MUA (Fig. 2, see also Materials and Methods for details). This method is based on a distance (or dissimilarity) matrix of the pairwise distances between multisite LFP or MUA time samples. For all seizures, this distance matrix had a diagonal block structure where the limits between two blocks correspond to the transitions between two consecutive stages (illustrated for the beginning of one seizure in Fig. 2B and 2D). Interestingly, the block structures based on LFPs and MUA differed, as assessed both from the results of our

algorithm and by visual inspection. These transitions could also be visualized in the original LFP and MUA time series (e.g. Fig. 2A and 2C). The transitions between two LFP stages were characterized by changes in their spectral content and/or morphology of epileptic discharges (Fig. 2A). On the other hand, the transitions between two MUA stages seemed to be associated with changes in MUA rate, amplitude and spatial distribution (Fig. 2C). We emphasize that this segmentation approach was used to define objectively the structure of LFP and MUA multichannel time series. Visual inspection was only used to verify the output of the algorithm and determine the finest scale at which to perform the segmentation.

We first applied this approach to the segmentation of MUA data from all seizures (illustrated for one seizure from each patient in Fig. 3). Our recordings contained two types of seizures, which we will refer to as spike-wave and gamma seizures (as reported previously e.g. in Truccolo et al., 2014). In spike-wave seizures (all patients except P5), we restricted our segmentation to the initial period of the seizure before rhythmic, stationary SWDs were established. In gamma seizures (P5), we segmented the entire seizures. In both cases, we defined local seizure onset as the time when the first epileptiform discharge could be seen in the LFPs, based on visual inspection. In all patients, we were successfully able to identify discrete stages characterizing the evolution of the multisite MUA rate over time (Fig. 3). To better understand the changes occurring between two consecutive stages, we examined the spatial distribution of the MUA rate averaged over time within each stage independently (illustrated for 3 different seizures in Fig. 4). In patient P1, the transitions between consecutive stages consisted mostly of spatially uniform variations in MUA rate. By contrast, in patients P2 and P3, the transitions were characterized by a profound reorganization in the spatial distribution of MUA rates. In patient P2, the regions of high MUA rate shifted from one corner of the MEA to another (e.g. Fig. 4, P2, between stages 5 and 6) before forming a collapsing wave (stages 6 to 8). In patient P3, variations in overall MUA rate (affecting the MEA uniformly) were accompanied by the presence of a first expanding wave (Fig. 4, P3, stages 4 to 6) followed by a collapsing wave (stages 6 to 8). We then systematically quantified the changes in overall MUA rate and degree of spatial reorganization (Fig. 5). The changes in spatial structure were assessed using the cosine distance, a measure that does not depend on the scale (or overall intensity) of the signals, i.e. two spatial patterns were considered similar if the differences between their respective MUA rates were spatially uniform (see Materials and Methods for more details). More precisely, we examined the evolution of the population MUA rate (averaged across electrodes) and of the cumulative cosine distance across successive stages (illustrated for P2, seizure1 in Fig. 5A). These two variables (population mean rate and cumulative cosine distance) fully characterized the changes occurring across successive stages. We used the population mean MUA rate as a function of the cumulative cosine distance as a way to summarize seizure evolution (illustrated in Fig. 5B for the 3 seizures presented in Fig. 4). We note that the obtained profiles are in good agreement with the visual assessment of the data in Fig. 4. For example, the changes in patient P1 are mostly characterized by variations in MUA rate with little spatial reorganization, as stated previously, while patients P2 and P3 had more profound changes in spatial patterns (compare the 3 profiles in Fig. 5B, which are all on the same scale for the cumulative cosine distance). Interestingly, these profiles were relatively consistent across seizures within each patient (Fig. 5C). There were two main exceptions in

patients P3 and P5. Seizure 1 from patient P3, which was shorter than the two other seizures as stated previously, nevertheless had a similar initial profile of evolution. It showed a large increase in the cumulative cosine distance during the last stage, which actually corresponded to the refractory period characterizing the end of the seizure. But the initial stages were similar between the three seizures. In patient P5, seizures 2 and 3 appeared very similar but seizure 1 diverged from this common profile after the first five stages. The original LFP and MUA time series revealed that seizure 1 contained a stage of intense MUA activity that was not present in the other seizures (Fig. 5D). Nevertheless, the evolutions before this stage of high activity were relatively similar. It is interesting that in these two patients (P3 and P5), some seizures appear as truncated versions of other seizures. Importantly, the existence of a common initial profile suggests similar mechanisms and local network dynamics during early propagation.

Next, we used LFPs instead of MUA to perform a similar analysis of the segmentation structure, changes in spatial patterns and consistency across seizures. This second analysis was important as segmentations based on LFPs and MUA can differ significantly as shown previously (Fig. 2). In place of the MUA rate, we considered the spectral power of LFPs in six frequency bands (delta: 0–2 Hz, theta: 2–8 Hz, alpha: 8–14 Hz, beta: 14–30 Hz, low-gamma: 30–60 Hz, mid-gamma: 60–90 Hz). The segmentation was based on all bands together, but we then examined the evolution across stages of each band independently (illustrated for 2 seizures and 3 bands on Fig. 6). As expected, we observed band-specific differences in the global spectral power and its temporal evolution, and major differences between spike-wave and gamma seizures. Remarkably, however, we noticed that the spatial patterns and their evolution over time were also band-specific. We summarized these evolutions using the same measures as before: the mean power across electrodes and the cumulative cosine distance between successive patterns of LFP power (Fig. 7). Similarly to the corresponding MUA analysis, we observed that the variations in mean power and spatial structure were quite consistent between seizures within each patient. One of the main exceptions, seizure 1 of patient P3, differed from the two other seizures in the same way as described previously in the MUA analysis. By contrast, in patient P5, the results slightly differed between the MUA and LFP analyses. The difference between seizure 1 and the other two seizures, obvious in the MUA segmentation, was subtler in terms of LFPs, visible only by the slight increase of power in the gamma bands during the second-last stage of the segmentation.

In summary, these results show that during the initial stages (tens of seconds after local seizure onset), seizures evolved through a succession of characteristic spatiotemporal patterns of MUA and LFPs, which were relatively consistent between seizures within each patient.

Individual SWDs and gamma oscillation cycles propagate with stage-dependent direction, speed and degree of directionality, independently of any ictal wavefront

We asked whether characteristic propagation patterns were also seen at the time scale of individual epileptic discharges (in spike-wave seizures) or gamma oscillation cycles (in gamma seizures), and how they were affected by the succession of the discrete stages

identified above. Spike-wave seizures were characterized by the presence of periodic phase-locked discharges in LFPs and MUA, called SWDs, which occurred at a frequency of 2–3 Hz. These discharges consisted of fast negative deflections in the LFPs (SWD 'spike' component), associated with strong MUA, followed by a period of neuronal spiking suppression with a more positive polarity in the LFPs ('wave' component). For each of these discharges, we first computed the relative delays between different electrodes and then extracted a directionality index, taking values between 0 and 1, where 0 corresponds to the absence of propagation and 1 represents a perfect plane wave (see Materials and Methods for more details). For discharges with a directionality index above a certain threshold (0.2), we also computed the average direction of propagation across the MEA. These analyses revealed that, in spike-wave seizures, many discharges propagated with stage-dependent propagation characteristics (illustrated for one seizure in Fig. 8). For example, in seizure 2 of patient P1, almost every LFP discharge clearly propagated during each stage after local seizure onset (Fig. 8A) and each stage was characterized by a specific direction of propagation and associated delay map (Fig. 8B). Remarkably, the direction of propagation changed dramatically across different stages of the seizure (especially between stages 2, 5 and 6). We also noticed that the same discharges were less directional when applying the same method to MUA instead of LFPs (Fig. 8C–D). These differences could be related to different physiological substrates underlying these two neural signals, or to the higher variance of MUA compared to LFPs. Nevertheless, when MUA discharges propagated with a directionality index above our threshold of 0.2, the directions of propagation of LFPs and MUA appeared similar (Fig. 8, compare A–B with C–D).

In gamma seizures, we investigated the propagation of gamma oscillation cycles (25–60 Hz) in both LFPs and MUA. We also noticed the presence of low-frequency (< 10 Hz) positive LFP discharges, in one particular stage common to all three seizures. Our analyses revealed that both gamma oscillations and low-frequency LFP discharges propagated (illustrated for one seizure in Fig. 9). In seizure 1 from patient P5, although we observed propagation (with a directionality index above 0.2) in all four stages of the seizure, the directions of propagation were consistent only during the last two stages (Fig. 9A–B, stages 3 and 4). The few low-frequency LFP discharges observed in stage 2 also propagated consistently. Interestingly, their directions of propagation were unrelated to the directions of propagation of gamma oscillations cycles seen in stages 3 and 4. Unlike in spike-wave seizures, MUA was very heterogeneous and the gamma band-filtered MUA rate (in 20-ms bins) did not show any clear propagation patterns (Fig. 9C, see low directionality indices, mostly below 0.2 in which case we did not compute the direction of propagation).

Finally, we investigated the characteristics of propagation during each stage and asked whether changes in these propagation patterns were associated with the presence of an ictal wavefront of increased MUA rate, as defined before. More precisely, we examined the directionality index, direction of propagation and speed of SWDs and gamma oscillations cycles during each stage of the segmented seizures, and we compared them to the population-averaged MUA rate (illustrated for one seizure in each patient on Fig. 10, and shown for all 15 seizures in Fig. S2). Overall, we observed that the propagation characteristics changed across seizure stages, but did not see any obvious correlation with the presence of an ictal wavefront. For example, the direction of propagation changed both

before and after the period of increased MUA in patient P1 (seizure 2), whereas the direction of propagation remained relatively constant throughout the seizure in patient P2 (seizure 2). In other cases, as in patients P3 (seizure 3) and P4 (seizure 2), there was not a clear direction of propagation in most of the seizure stages. In patient P5 (seizure 1), we observed propagation of gamma oscillation cycles only after the occurrence of low-frequency LFP discharges, but no ictal wavefront was present in this type of seizure. Similarly, no clear correlation was seen between the presence of an ictal wavefront and the speed or directionality index. Interestingly, in the two patients with the most pronounced propagation, the propagation patterns were also consistent across seizures (Fig. S2, patients P1 and P2).

DISCUSSION

This study presented three main findings. First, we have shown that LFP and MUA signals evolved through discrete stages during early seizure propagation in neocortex. Segmented early seizure stages based on LFPs or MUA showed a dissociation of their spatiotemporal dynamics, but tended to be consistent within each patient. Even when a seizure diverged from the most common pattern in a given patient, the initial stages (corresponding to what we call the early propagation) were nevertheless similar, and the divergence occurred later once the seizure was already established. Second, although some seizures were characterized by a single peak in MUA rate that occurred several seconds after local seizure onset, other seizures had a more complex structure reflecting recruitment mechanisms which might be different from a simple ictal wavefront. Finally, LFP paroxysmal discharges and/or gamma oscillations (depending on the type of the seizure) propagated across the MEA even before the MUA build-up (when such a build-up was observed), and had stage-specific propagation characteristics.

Succession of discrete seizure stages from spatiotemporal LFPs and MUA

In most previous studies, the dynamics of seizure transitions in neocortex have been studied extensively using macroscale recordings, either from electroencephalography (EEG) or electrocorticography (ECoG), showing distinct dynamics during the initiation, evolution and termination of seizures at the macroscale resolution (Schiff et al., 2005; Schindler et al., 2007; Kramer et al., 2012; Wulsin et al., 2014). On the other hand, microscale recordings using MEAs have revealed important differences between population synaptic activity (reflected in LFPs) and local neuronal firing. In particular, Schevon and colleagues (Schevon et al., 2012; Weiss et al., 2013) suggested that strong phase-locking between these two types of signals might be an indicator of local recruitment into a seizure. Here, we show the first MUA-based segmentation of seizure early propagation into reproducible discrete stages, before phase-locking between LFPs and MUA emerges, or even in the absence of such phase-locking. These results open a new perspective on the early propagation of seizures, where neocortical territories are not simply recruited into the seizure but undergo a succession of consistent, spatially organized changes in spiking activity, sometimes (but not necessarily) leading to synchronized discharges with phase-locked LFPs and MUA. The reproducibility of these stages might also have important implications for the development of closed-loop systems for seizure control.

At first sight, the fact that seizures evolve through discrete stages at the microscopic level might not seem unexpected given that macroscopic EEG or ECoG signals also show distinct stages, with changes in amplitude or frequency throughout the seizure (e.g. Schiff et al., 2005). However, it was surprising to observe some level of dissociation between the segmentations based on LFPs and MUA. This dissociation was apparent in the number of identified stages and in the timing of the transitions between two consecutive stages. We believe such dissociation is due to LFPs and MUA reflecting, respectively, synaptic activity due to (local and non-local) inputs versus local network spiking activity. In essence, the former is often thought as largely related to averaged subthreshold activity while the latter a measure of neuronal output. Combining information from these two types of signals could yield more information about neural state transitions, both locally and distally to the recording site. An interesting follow-up study would be to determine whether transitions in spiking activity (MUA) actually explain or result from transitions in LFPs, and whether this causal relationship varies with the recording location (inside or outside the seizure onset zone).

Another interesting observation is the presence of stage-specific patterns in the spatial distribution of MUA and bandpass-filtered LFPs (alpha, beta, etc). In some patients, the spatial distribution of MUA across successive stages suggested complex but organized and consistent propagation patterns. Notably, these patterns appeared to be more complex than plane waves, with some examples of collapsing or expanding waves. Although we think that these patterns reflect mostly the complex structure of local synaptic inputs, and potentially the presence of patchy connections (as illustrated e.g. by Wang et al., 2014), we cannot entirely rule out the possible contribution of different recording layers. Due to the curvature of the brain or MEA insertion issues, some of the microelectrodes could have recorded from different cortical layers. We expect future studies combining structural MRI and more detailed histology to address this issue. Comparing seizure progression at this microscopic scale with simultaneous ECoG recordings registered with MRI might also help to elucidate the evolution of these local spatiotemporal patterns.

Finally, these patterns were relatively consistent within a given patient, but not across patients, which is not surprising given the differences in etiology, seizure onset zone and electrode location among these patients. Within patients, we observed very reproducible stages in 3 of the 5 patients. In the two other patients, the initial stages were always consistent, but the later stages could diverge. More precisely, some seizures appeared as shorter, truncated versions of the most common pattern, reflecting perhaps the operation of different seizure termination mechanisms.

Ictal wavefront and seizure recruitment

Few studies have investigated human seizure propagation at the microscale level (Schevon et al. 2010, 2012; Truccolo et al. 2011, 2014). In one of these studies, Schevon et al. (2012) proposed a model based on a dissociation between cortical regions that have been recruited or not into a seizure, respectively called the core territory and ictal penumbra. According to this model, the non-recruited regions (ictal penumbra) would show low-level spiking activity non phase-locked with large amplitude EEG or LFP discharges. Once these regions

are recruited into the seizure (due to a failure in an hypothesized inhibitory veto to seizure spread), neuronal firing would become transiently very high, defining an ictal wavefront propagating at a slow speed (0.12–0.26 $mm.s^{-1}$), followed by rhythmic multiunit activity phase-locked to large-amplitude and low-frequency LFP discharges.

In the 4 patients with spike-wave seizures we did observe periods of transient MUA build up. In 2 of these 4 patients however, some MEA recording sites showed the presence of two, and not one, periods of increased MUA. Furthermore, although the largest MUA peak usually preceded periods of stationary and rhythmic activity with phase-locked LFPs and MUA, that was not always the case. In one of the examined spike-wave seizures, the MUA peak occurred after the emergence of 2–3Hz spike-wave discharges with LFP-MUA phase-locked activity, which were already present during previous stages, in disagreement with the model of the ictal wavefront described above. In addition, these MUA peaks did not always have clear propagation patterns. We note, nevertheless, that differences between our findings and those of Schevon et al. (2012) could have potentially originated from differences in the particular seizure onset areas and their relationship (e.g. connectivity) with the area of propagation recorded by the implanted MEA in the studied patients.

Our results also indicate that the period preceding the phase-locking mechanism between LFPs and MUA in spike-wave seizures has a very rich spatiotemporal structure, both in LFPs and MUA, with multiple stages of characteristic neural states. As stated above, the initial stages (corresponding to the early propagation of the seizure) were relatively consistent within a given patient, even if some seizures could diverge from the most common pattern during the later stages. Therefore, we think that the description of seizure recruitment and early propagation using stage segmentation framework adopted here leads to a more complex picture of ictal dynamics than the hypothesis of a simple propagating ictal wavefront.

In one patient (P5), seizures had a very different electrophysiological signature, characterized by sustained narrowband gamma oscillations. These seizures showed no clear MUA peaks. We stress that in all patients, the MEA was located a few centimeters outside the seizure onset zone as defined by a neurologist in the clinical team, and ECoG grids covered an area that included the seizure onset zone. It is also important to note that all seizures presented in this study were defined as clinical, i.e. with obvious behavioral correlates. We think the differences between the patient with gamma seizures and other patients with spike-wave seizures are related to the etiology of the disorder rather than differences in electrode location. The different dynamics seen among these patients might also reflect different mechanisms in different seizure types (e.g. Salami et al., 2015), rather than a single mechanism based on feedforward inhibitory veto. Computational studies have also shown that different types of spatiotemporal dynamics, with or without propagation of a smooth or patchy wavefront, can be obtained within the same model, using different sets of parameters presumably corresponding to distinct pathophysiological mechanisms (Wang et al., 2014). In addition, transient elevation of fast spiking inhibitory neurons can play different roles, in some cases actually contributing to seizure initiation as shown, for example, by Uva et al. (2015). More detailed studies based on the classification of single units into putative excitatory and inhibitory cells (e.g. Truccolo et al., 2011; Ahmed et al.,

2014) are necessary to examine how slow transient increases in MUA observed in spike-wave seizures are related to inhibitory activity.

Microscale propagation of paroxysmal discharges and gamma oscillations

After examining seizure evolution at a timescale on the order of several seconds (MUA peaks and segmentation into successive stages), we investigated the spatiotemporal dynamics of individual epileptic discharges or gamma oscillations occurring at a finer timescale, i.e. oscillatory events with periods of ~ 200–300 ms for SWDs and ~ 20–30 ms for gamma oscillations. In spike-wave seizures, we found clear LFP cortical waves (as also reported recently by González-Ramírez et al., 2015), which propagated with similar speeds during most seizure stages, not only during but also before the stages that followed MUA peaks. Additionally, we found no clear correlation across patients between the changes in LFP propagation patterns and the occurrence of the MUA peak. A similar analysis of the propagation patterns based on MUA was more challenging, presumably because of the higher temporal variability of MUA signals compared to LFPs. Nevertheless, high-amplitude MUA discharges during spike-wave seizures, likely reflecting more synchronized neuronal spiking, had propagation patterns similar to the ones obtained from LFPs during the same time period. These discharges tended to occur during and after the MUA peak (i.e. “ictal wavefront”) period. This was not true for gamma seizures, in which MUA did not seem to exhibit any clear or consistent propagation patterns. More detailed analyses of the relationship between LFP and MUA wave propagation during spike-wave discharges, including time causal analysis, is a topic for future studies.

CONCLUSIONS

In summary, we have shown that: (1) the period of early seizure propagation in neocortex is characterized by a succession of consistent, discrete stages in LFPs and MUA. (2) In spike-wave seizures, these stages are usually associated with the presence of one or more peaks in the MUA rate, which precede in most cases the emergence of phase-locked discharges between LFPs and MUA. (3) Each of these stages has intrinsic spatiotemporal dynamics, which influence the propagation patterns of individual spike-wave discharges or gamma oscillations occurring at a much finer time resolution, but without any clear relationship with the presence of an MUA peak. We also think that the analyses based on multiple discrete stages and segmentation framework adopted here will have practical implications for the development of closed-loop systems for seizure control, allowing, for example, a stage-dependent optimization of the stimulation parameters.

Supplementary Material

Refer to Web version on PubMed Central for supplementary material.

Acknowledgments

We would like to thank the patients who participated in this study, the nursing and medical staff at Massachusetts General and Rhode Island Hospitals, Omar Ahmed and other members of the Cash lab for helping with data recordings, and Michael Rule for suggesting the use of the similarity matrix for seizure segmentation. This research was supported by: the National Institute of Neurological Disorders and Stroke (NINDS), grants R01NS079533 (to WT), R01NS062092 (to SSC); the Department of Veterans Affairs, Merit Review Award RX000668-01A2, (to

WT); and the Pablo J. Salame 88 Goldman Sachs endowed Assistant Professorship of Computational Neuroscience (WT).

References

Ahmed, O.; Kramer, M.; Truccolo, W.; Naftulin, J.; Potter, N.; Eskandar, N.; Cosgrove, G.; Blum, A.; Hochberg, L.; Cash, S. Inhibitory single neuron control of seizures and epileptic traveling waves in humans. Computational Neuroscience Meeting; Quebec City. 2014.

Cacioppo S, Weiss RM, Runesha HB, Cacioppo JT. Dynamic spatiotemporal brain analyses using high performance electrical neuroimaging: theoretical framework and validation. J Neurosci Methods. 2014; 238:11–34. [PubMed: 25244954]

González-Ramírez LR, Ahmed OJ, Cash SS, Wayne CE, Kramer MA. A biologically constrained, mathematical model of cortical wave propagation preceding seizure termination. PLoS Comput Biol. 2015; 11:e1004065. [PubMed: 25689136]

Hochberg LR, Serruya MD, Friehs GM, Mukand JA, Saleh M, Caplan AH, Branner A, Chen D, Penn RD, Donoghue JP. Neuronal ensemble control of prosthetic devices by a human with tetraplegia. Nature. 2006; 442:164–171. [PubMed: 16838014]

Keller CJ, Truccolo W, Gale JT, Eskandar E, Thesen T, Carlson C, Devinsky O, Kuzniecky R, Doyle WK, Madsen JR, Schomer DL, Mehta AD, Brown EN, Hochberg LR, Ulbert I, Halgren E, Cash SS. Heterogeneous neuronal firing patterns during interictal epileptiform discharges in the human cortex. Brain. 2010; 133(Pt 6):1668–1681. [PubMed: 20511283]

Kramer MA, Truccolo W, Eden UT, Lepage KQ, Hochberg LR, Eskandar EN, Madsen JR, Lee JW, Maheshwari A, Halgren E, et al. Human seizures self-terminate across spatial scales via a critical transition. Proc Natl Acad Sci USA. 2012; 109(51):21116–21121. [PubMed: 23213262]

Mitra, P.; Bokil, H. Observed Brain Dynamics. Oxford; New York: Oxford University Press; 2007.

Morrell MJ. On behalf of the RNS System in Epilepsy Study Group. Responsive cortical stimulation for the treatment of medically intractable partial epilepsy. Neurology. 2011; 77(13):1295–1304. [PubMed: 21917777]

Rubino D, Robbins KA, Hatsopoulos NG. Propagating waves mediate information transfer in the motor cortex. Nat Neurosci. 2006; 9:1549–1557. [PubMed: 17115042]

Salami P, Lévesque M, Gotman J, Avoli M. Distinct EEG seizure patterns reflect different seizure generation mechanisms. J Neurophysiol. 2015; 113:2840– 2844. [PubMed: 25652916]

Schevon CA, Goodman RR, McKhann G, Emerson RG. Propagation of epileptiform activity on a submillimeter scale. J Clin Neurophysiol. 2010; 27(6):406–411. [PubMed: 21076338]

Schevon CA, Ng SK, Cappell J, Goodman RR, McKhann G, Waziri A, Branner A, Sosunov A, Schroeder CE, Emerson RG. Microphysiology of epileptiform activity in human neocortex. J Clin Neurophysiol. 2008; 25(6):321–330. [PubMed: 18997628]

Schevon CA, Weiss SA, McKhann G, Goodman RR, Yuste R, Emerson RG, Trevelyan AJ. Evidence of an inhibitory restraint of seizure activity in humans. Nat Commun. 2012; 3:1060. [PubMed: 22968706]

Schiff SJ, Sauer T, Kumar R, Weinstein SL. Neuronal Spatiotemporal Pattern Discrimination: The Dynamical Evolution of Seizures. Neuroimage. 2005; 28(4):1043–1055. [PubMed: 16198127]

Schindler K, Leung H, Elger CE, Lehnertz K. Assessing seizure dynamics by analysing the correlation structure of multichannel intracranial EEG. Brain. 2007; 130:65–77. [PubMed: 17082199]

Thurman DJ, Beghi E, Begley CE, Berg AT, Buchhalter JR, Ding D, Hesdorffer DC, Hauser WA, Kazis L, Kobau R, et al. Standards for epidemiologic studies and surveillance of epilepsy. Epilepsia. 2011; 52(Suppl 7):2–26. [PubMed: 21899536]

Truccolo W, Friehs GM, Donoghue JP, Hochberg LR. Primary motor cortex tuning to intended movement kinematics in humans with tetraplegia. J Neurosci. 2008; 28(5):1163–1178. [PubMed: 18234894]

Truccolo W, Hochberg LR, Donoghue JP. Collective dynamics in human and monkey sensorimotor cortex: predicting single neuron spikes. Nat Neurosci. 2010; 13:105–111. [PubMed: 19966837]

Truccolo W, Donoghue JA, Hochberg LR, Eskandar EN, Madsen JR, Anderson WS, Brown EN, Halgren E, Cash SS. Single-neuron dynamics in human focal epilepsy. Nat Neurosci. 2011; 14:635–641. [PubMed: 21441925]

Truccolo W, Ahmed OJ, Harrison MT, Eskandar EN, Cosgrove GR, Madsen JR, Blum AS, Potter NS, Hochberg LR, Cash SS. Neuronal ensemble synchrony during human focal seizures. J Neurosci. 2014; 34(30):9927–9944. [PubMed: 25057195]

Uva L, Breschi GL, Gnatkovsky V, Taverna S, de Curtis M. Synchronous inhibitory potentials precede seizure-like events in acute models of focal limbic seizures. J Neurosci. 2015; 35(7):3048–3055. [PubMed: 25698742]

Wang Y, Goodfellow M, Taylor PN, Baier G. Dynamic mechanisms of neocortical focal seizure onset. PLoS Comput Biol. 2014; 10:e1003787. [PubMed: 25122455]

Waziri A, Schevon CA, Cappell J, Emerson RG, McKhann GM, Goodman RR. Initial surgical experience with a dense cortical microarray in epileptic patients undergoing craniotomy for subdural electrode implantation. Neurosurgery. 2009; 64(3):540–545. [PubMed: 19240617]

Weiss SA, Banks GP, McKhann GM, Goodman RR, Emerson RG, Trevelyan AJ, Schevon CA. Ictal high frequency oscillations distinguish two types of seizure territories in humans. Brain. 2013; 136(Pt 12):3796–3808. [PubMed: 24176977]

Wulsin DF, Fox EB, Litt B. Modeling the complex dynamics and changing correlations of epileptic events. Artificial Intelligence. 2014; 216:55–75. [PubMed: 25284825]

Highlights

- Neocortical propagation of human focal seizures involves successive discrete stages.
- Each stage has a characteristic evolution in overall activity and spatial patterns.
- LFP and multi-unit activity show different stage sequences and evolution.
- Seizures can show single or multiple multi-unit activity peaks after seizure onset.
- Spike-wave discharges and (~40 Hz) gamma cycles propagate in stage-specific ways.

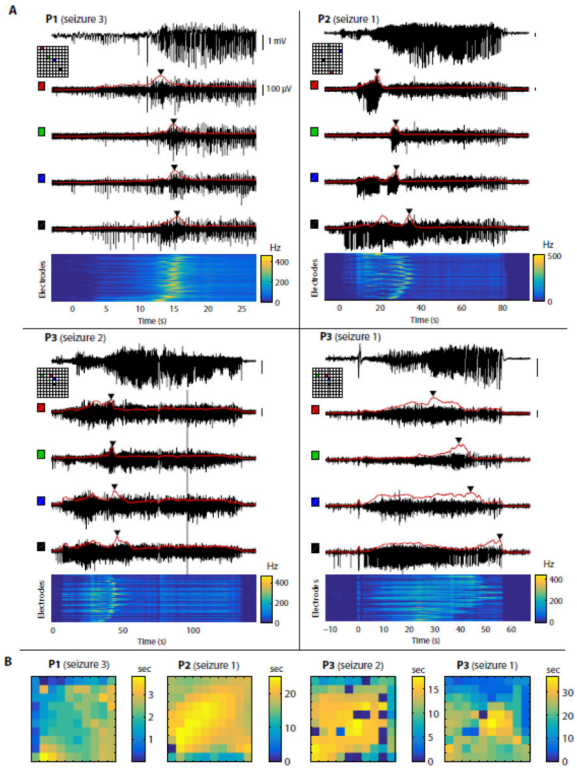

Figure 1. Seizure propagation dynamics are complex and variable across patients

(A) Each panel represents a different patient/seizure. On each panel, the top trace shows LFPs (0.3–300 Hz) recorded from a representative electrode. The 4 black traces below show high-pass MUA (300 Hz – 7.5 kHz) from 4 electrodes located on the MEA at the positions indicated on the corresponding map (each electrode is associated with a color shown both on the map and next to the corresponding trace). The red curve overlaid with each MUA trace shows the rate of thresholded MUA (4 standard deviations above or below the mean, binned in 1-s overlapping time windows). Triangular markers indicate the time when the MUA rate reaches a maximum on each electrode. At the bottom, the heat map represents the MUA rate over time (x-axis) and across electrodes (y-axis, ordered row-wise across the MEA). **(B)** Delay maps of the peak of MUA rate. For each example shown in (A), the peak of MUA rate on each electrode was identified, and the latency with respect to the earliest electrode was plotted as a heat map. The 1st example (P1, seizure 3) reveals propagation resembling a plane wave, but the 3 other examples show more complex or unclear propagation patterns.

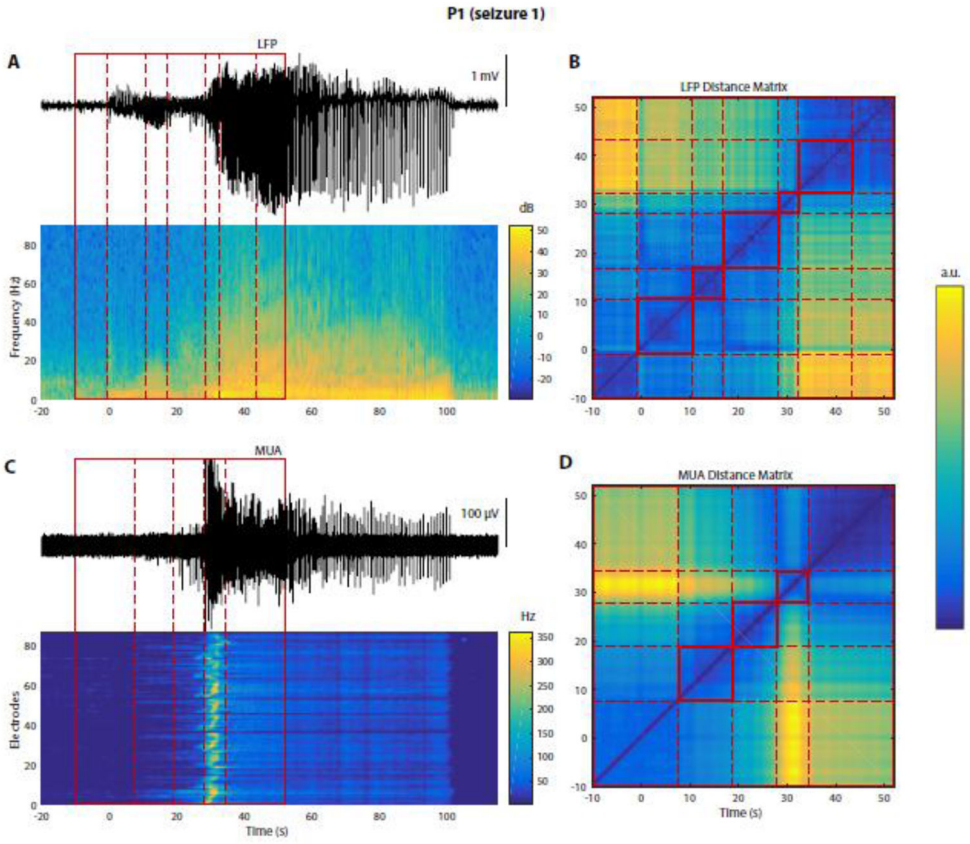

Figure 2. Seizures can be segmented into distinct stages based on LFPs or MUA

All data on this figure are from P1, seizure 1. **(A)** Top trace: LFPs from a representative electrode. Heat map below: corresponding multitaper spectrogram (see Materials and Methods). Red box (solid lines): time period manually selected for segmentation, encompassing seizure onset (indicated by t = 0 s, based on visual inspection). Dashed red lines: results of a semi-automatic segmentation algorithm (see Materials and Methods) applied on LFPs, and dividing the seizure into different stages. **(B)** LFP-based distance matrix used by the segmentation algorithm to find transitions between different segments/stages. Each axis: time period within the red box in (A). The color of each point (t_i, t_j) represents the "distance", or dissimilarity, between the multichannel LFPs recorded at the two times t_i and t_j, based on spectral features obtained from LFPs. Dashed red lines: limits of the different stages found by the algorithm, and also shown in (A). **(C)** Top trace: high-pass MUA from the same electrode as in (A). Heat map: MUA rate (in 1-s bins) over time (x-axis) and across electrodes (y-axis, ordered row-wise across the MEA). Red box: same as in (A). Dashed red lines: results of the segmentation algorithm applied to MUA data. Note the differences between the segmentations based on LFPs and MUA. **(D)** MUA-based distance matrix used by the segmentation algorithm. This panel is similar to (B) but with features derived from MUA instead of LFPs.

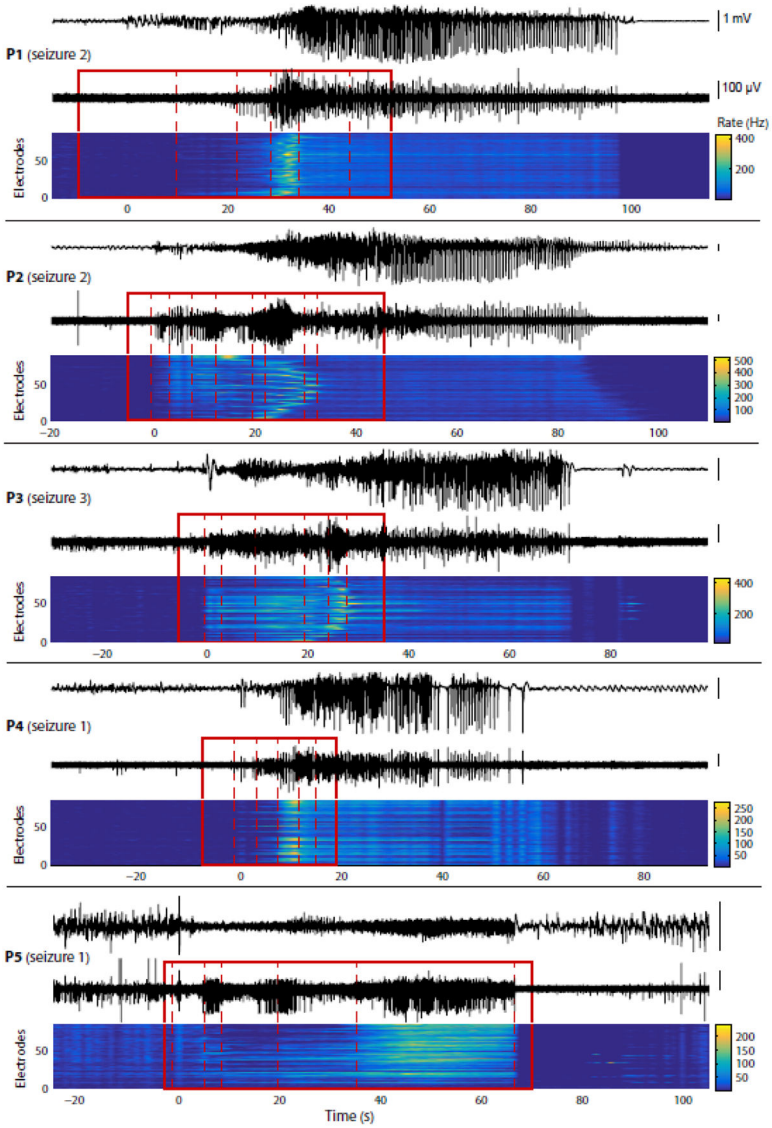

Figure 3. Segmentation of the seizure early propagation period reveals successive MUA dynamics in all patients

MUA-based segmentation during seizure early propagation, similar to Fig. 2C, applied to 1 seizure in each of the 5 patients (top and bottom traces: respectively LFPs and high-pass MUA from same electrode; heat map: MUA rate across electrodes). The first 4 patients had spike-and-wave seizures, while the last patient (P5) had gamma seizures. Note that the maximum in MUA rate occurs within a single stage in two patients (P1 and P4) but is distributed across several distinct stages in two other patients (P2 and P3). In the patient with gamma seizures (P5), no peak in MUA rate is apparent but a structure composed of discrete stages can still be identified. Overall, a succession of discrete stages each characterized by its own MUA dynamics is observed in all patients/seizures, but this structure is not the same across patients.

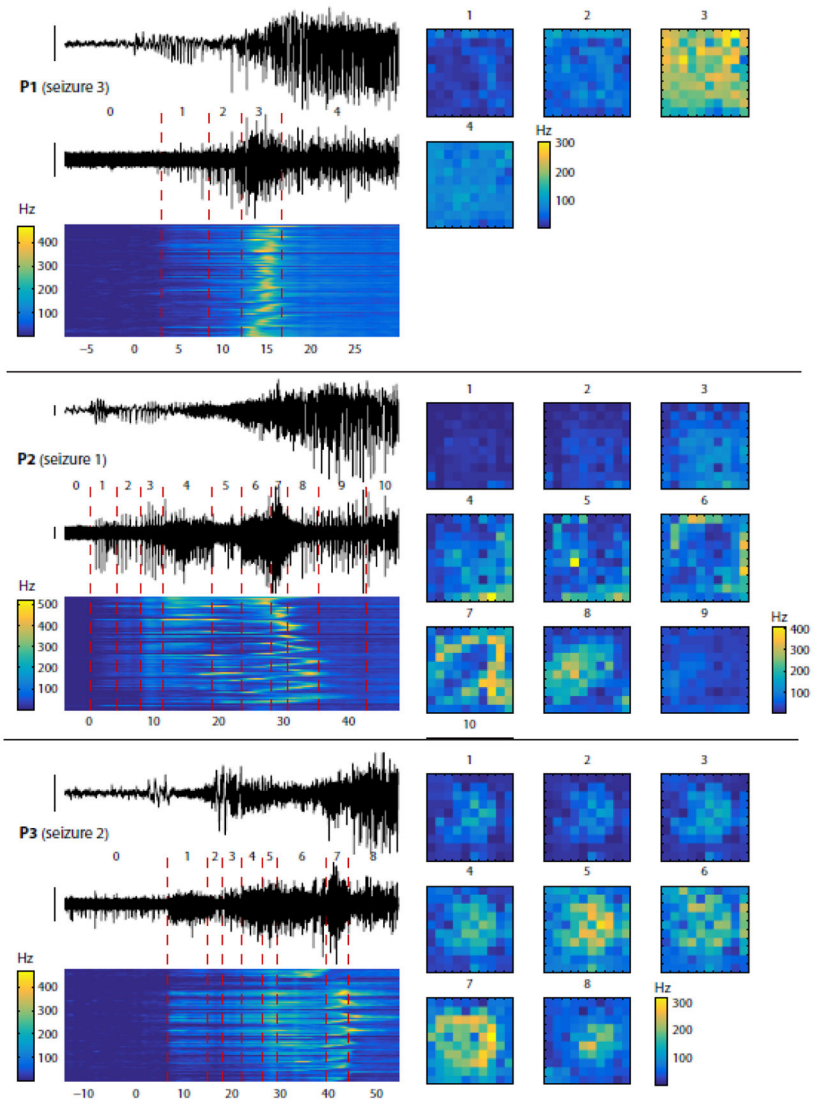

Figure 4. MUA dynamics during each stage of seizure early propagation are associated with particular spatial patterns and overall population activity

Each panel represents one patient/seizure (top to bottom: P1, seizure 3; P2, seizure 2; P3, seizure 2), selected to illustrate the variability of the observed MUA spatial patterns (quantification across all seizures is performed in Fig. 5). In each panel, the left part is similar to Fig. 3 (two traces: LFPs and high-pass MUA from same electrode; heat map: MUA rate across electrodes; different stages numbered 0, 1, etc., 0 being the last stage before seizure onset). The right part shows the MUA rate during each stage, averaged over time, and represented as a spatial map of the 10×10 MEA. Missing electrodes were interpolated (see Materials and Methods). In the 1st example (P1), the variations of MUA rate affect the MEA almost uniformly, while more complex spatial structures can be observed in the 2nd and 3rd examples (P2 and P3).

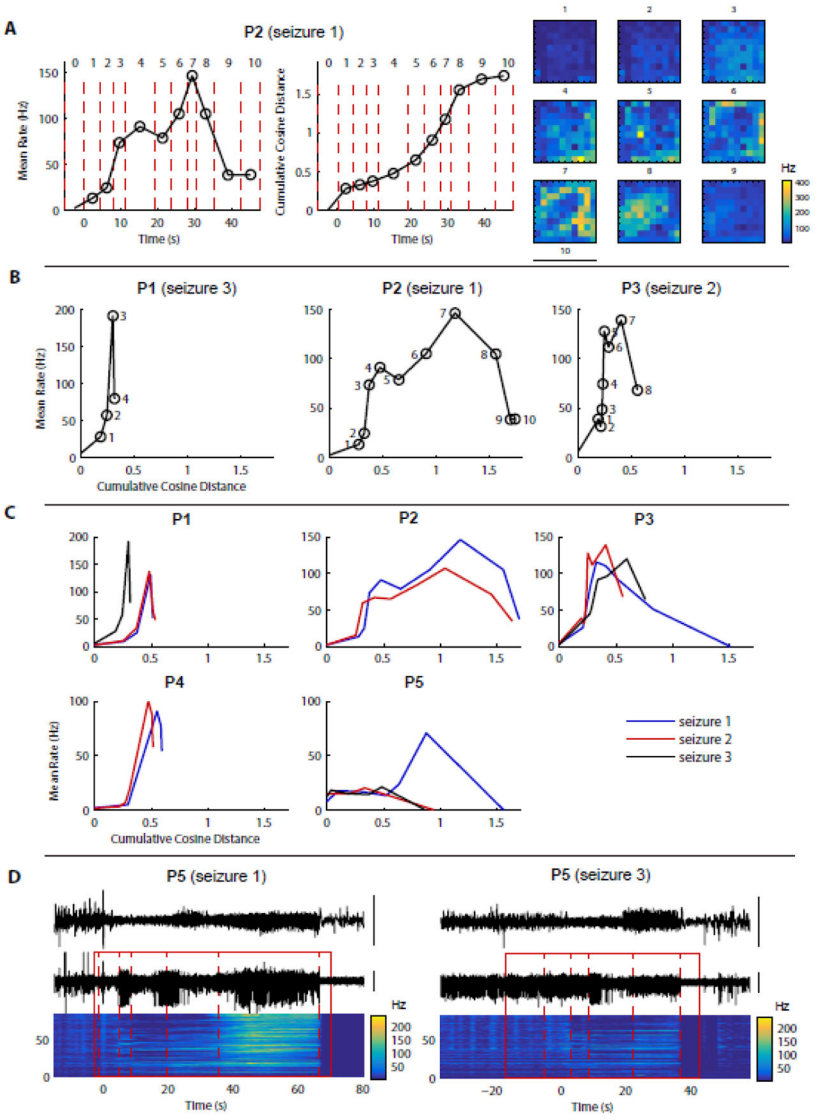

Figure 5. MUA population activity and spatial patterns change across stages but their evolution is similar within a given patient

(A) Data in this panel are from the 2nd example shown in Fig. 4 (P2, seizure 1). Left: population mean rate over time. Each dot: MUA rate averaged over time and across electrodes during the corresponding stage of the segmented seizure (numbered 0, 1, etc., 0 being the last stage before seizure onset). Middle: cumulative cosine distance over time. Each dot: cumulative cosine distance of the MUA rate maps between the stage where the dot is represented and the preceding stage. The cosine distance is used to compare MUA rate maps independently of the population overall activity (see Materials and Methods for more details). Right: corresponding MUA rate maps (from Fig. 4, P2) shown as a reminder. **(B)** Condensed representation of seizure evolution: for each example shown in Fig. 4, the population mean MUA rate is plotted as a function of the cumulative cosine distance introduced in (A). The coordinates of each dot show the cumulative cosine distance and the population mean MUA rate during one stage of the seizure (stage numbers indicated next to

each dot). **(C)** Same representation as in (C) but for all seizures from each patient. These "signatures" of seizure evolution are relatively consistent within each patient. The most important exceptions are seizure 1 from P3 and seizure 1 from P5. **(D)** LFP and MUA data for 2 seizures from patient P5, where the biggest variability between seizures was observed in (C).

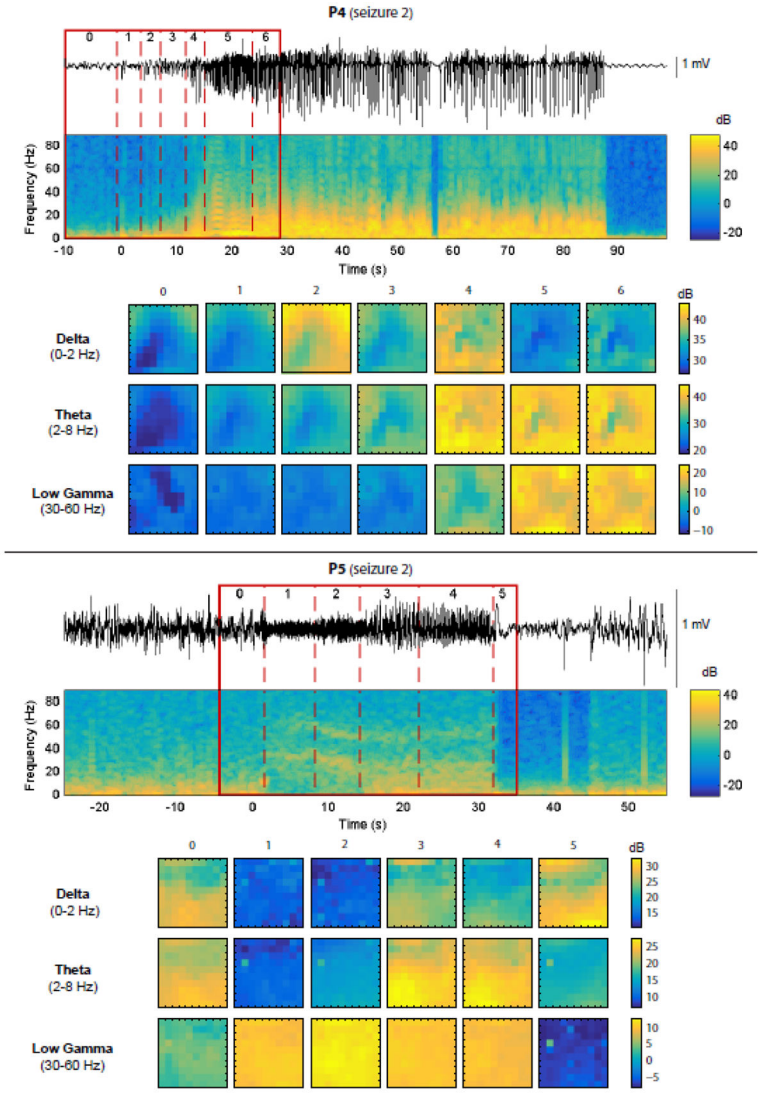

Figure 6. LFP frequency bands are also associated with specific powers and spatial patterns during each stage of seizure early propagation

Each panel represents one patient/seizure (top: P4, seizure 2; bottom: P5, seizure 2). In each panel, the top part shows the LFPs from 1 representative electrode, the corresponding spectrogram and the results of the segmentation algorithm based on LFPs (as described already in Fig. 2). The bottom part shows the LFP power in different frequency bands (delta, theta, low-gamma; chosen to emphasize diversity in the recorded signals) during each stage, averaged over time, and represented as a spatial map of the 10×10 MEA. Missing electrodes were interpolated (see Materials and Methods). In both the spike-and-wave seizure (P4, top) and the gamma seizure (P5, bottom), variations in overall LFP power and in spatial structure can be observed across stages, with differences related to the frequency band and seizure type.

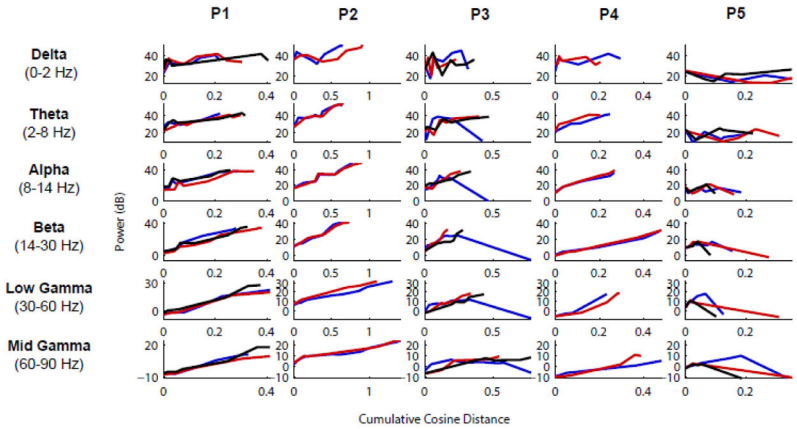

Figure 7. Band-specific LFP power and spatial patterns change across stages but their evolution is similar within a given patient

For each frequency band investigated (delta, theta, alpha, beta, low-gamma, mid-gamma) and each patient, the variations in LFP overall power and spatial structure were quantified similarly to the MUA (Fig. 5C). Specifically, the y-axis shows the electrode- and time-averaged band-filtered LFP power during each stage, and the x-axis shows the cumulative cosine distance between the band-filtered LFP power maps across consecutive stages. With only a few exceptions, the profiles are very similar among seizures within the same patient, as also shown before based on MUA analysis (Fig. 5). We note also a general increase in power throughout seizure early propagation, and a larger degree of spatial reorganization in high frequencies compared to low frequencies.

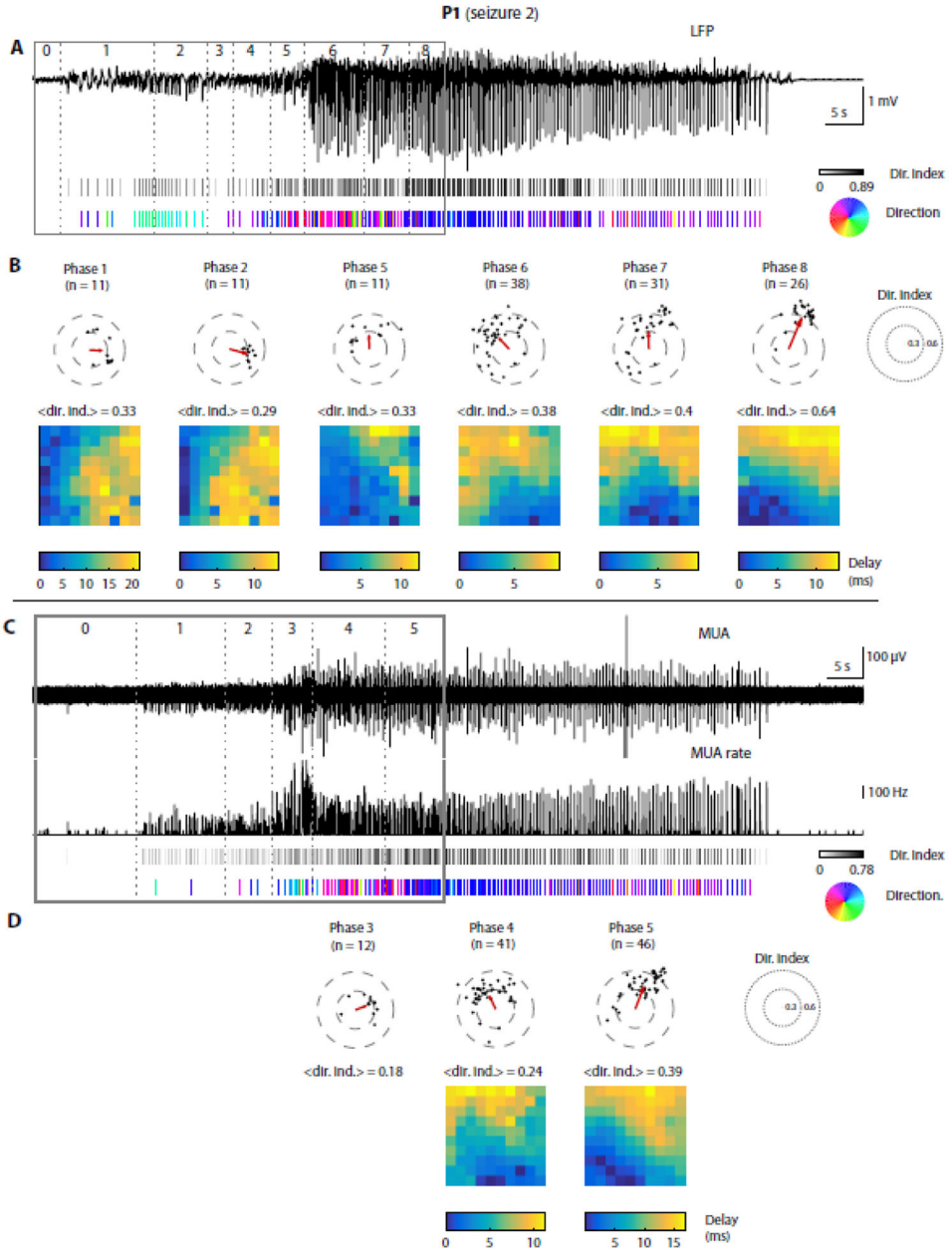

Figure 8. LFP and MUA discharges propagate in a stage-specific manner during a spike-wave seizure.<

br>Data from P1, seizure 2. **(A)** Top trace: LFPs from a representative electrode. Solid and dotted lines: segmented seizure as before. 1st raster below: each tick represents one LFP discharge; its color indicates the directionality index (see Materials and Methods), ranging from 0 (white, no directionality) to 1 (black, strong directionality). 2nd raster: directions of propagation for discharges with a directionality index greater than 0.2, color-coded according to the hue wheel shown on the right. **(B)** Summary within each stage of seizure early propagation (only the 6 most interesting stages are represented, one per vertical panel). Scatter plot: each dot represents one LFP discharge, with its directionality index and direction of propagation as polar coordinates. Only discharges with a directionality index

above 0.2 are shown. Red arrow: circular average propagation vector. <dir. ind.>: average directionality index across all discharges (both above and below 0.2). Below: average delay map for discharges with a directionality index above 0.2; a 0-ms delay corresponds to the electrode with the shortest average latency with respect to the population peak. **(C–D)** Similar analysis as shown in (A–B), based on MUA instead of LFPs. In (C), the 1st and 2nd traces show respectively the high-pass MUA and thresholded MUA rate in 20-ms bins (time resolution chosen to isolate individual discharges). The rest of the analysis is the same as in (A–B) using peaks in the MUA rate instead of LFPs.

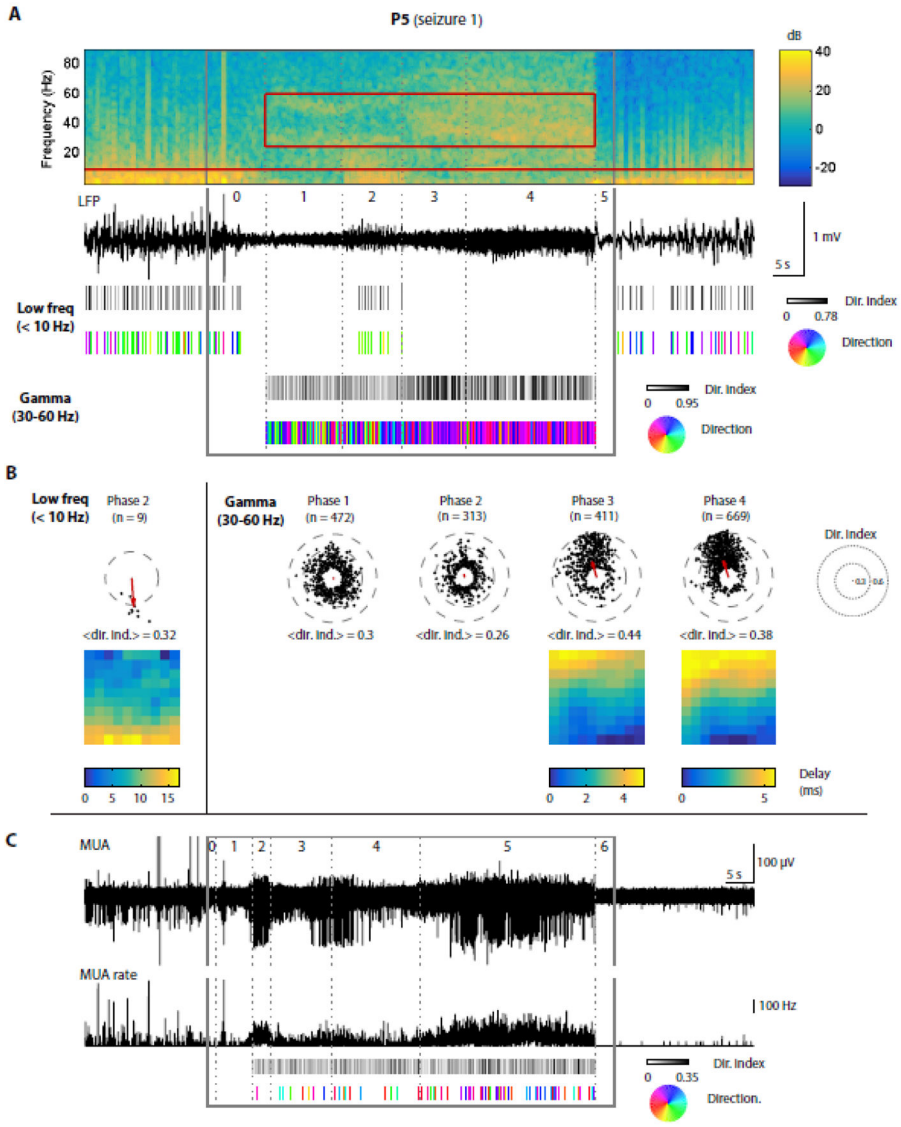

Figure 9. LFP discharges and gamma oscillations propagate in a stage-specific manner during a gamma seizure

Similar to Fig. 8 but for a gamma seizure: data from P5, seizure 1. **(A)** At the top, the LFP spectrogram and corresponding trace from a representative electrode show two different features of this gamma seizure: an overall increase in gamma power between stage 2 and stage 5 (25–60 Hz, red rectangle on spectrogram), and low-frequency discharges (< 10 Hz, below red horizontal line on spectrogram) occurring during stage 3 exclusively. Below, the directionality index and direction of propagation are shown as rasters (as in Fig. 8) for low-frequency discharges and for gamma oscillations independently. For gamma oscillations, each tick represents a peak in the gamma LFPs filtered between 25 and 60 Hz; results are shown only during stages 2 to 5 where the gamma power was increased based on visual inspection. **(B)** Similar to Fig. 8B, shown independently for low-frequency discharges and gamma oscillations. Note that the propagation patterns of gamma oscillations are unclear during stages 1 and 2, but become more directional and consistent during stages 3 and 4. **(C)**

Similar to Fig. 8C, with the exception that we filtered the MUA rate in the gamma range (25–60 Hz) before computing the directionality index and direction of propagation (the bottom trace shows the MUA rate before filtering). Since there is no clear propagation in terms of gamma-MUA in this patient/seizure, we did not perform a summary for each stage as we did for LFPs.

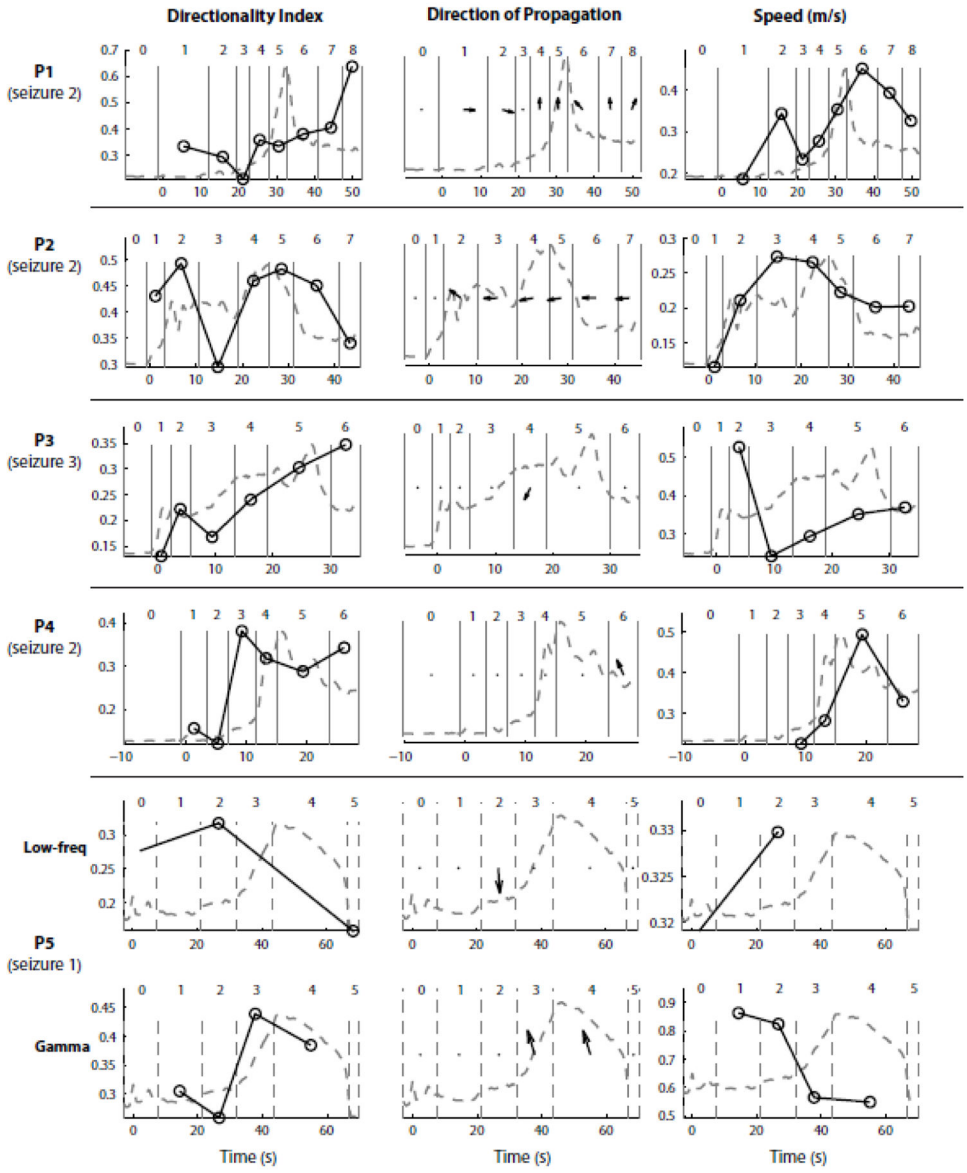

Figure 10. Propagation characteristics of LFP discharges and gamma oscillations do not reveal a strong association with MUA rate peak events

This figure summarizes across all patients the analyses of propagation already illustrated in Figs. 8 and 9. Each row corresponds to one selected seizure in each patient. Columns 1, 2 and 3 represent respectively the evolution over time of the LFPs directionality index, direction of propagation and speed (black circles and solid line). Each circle corresponds to the average directionality index, average direction of propagation or average speed during a specific stage of the seizure (stage boundaries indicated by vertical gray lines and numbered as before). The directionality index was averaged across all LFP discharges or gamma oscillations. The direction of propagation and speed were averaged only across discharges/ gamma oscillations with a directionality index above 0.2 (Material and Methods). A dot indicates that the average directionality vector had a norm below 0.2 or that the total number of discharges/gamma oscillations used to compute the average was smaller than 3, meaning

that the average direction of propagation was unclear. The dashed grey line represents the population MUA rate, obtained by averaging the MUA rate (in 1-s bins) across electrodes and represented in arbitrary units. This trace shows the temporal location/profile of the MUA rate peak. Overall, we observe no clear relationship between the characteristics of propagation and MUA rate peak events (“ictal wavefront”).